Modulating the Mucosal Drug Delivery Efficiency of Polymeric Nanogels Tuning their Redox Response and Surface Charge

Jakes Udabe, Amanda Muñoz-Juan, Belal Tafech, María Soledad Orellano, Sarah Hedtrich, Anna Laromaine, and Marcelo Calderón*

Mucus is a hydrated, viscoelastic, and adhesive gel that lubricates and protects the body from pathogens; however, its protective function hinders drug/nanomedicine diffusion and treatment efficiency. Therefore, novel drug delivery strategies are required to overcome challenging mucosal barriers. Here, multi-responsive nanogels (NGs) are developed and explored their interaction with mucus. Specific NG features (e.g., surface charge, temperature responsiveness, and redox response) are evaluated in a typical mucus-associated environment (i.e., mucin proteins and high glutathione concentrations). The results demonstrate that biocompatibility and the capacity to deliver a protein through mucosal barriers in different in vitro and in vivo models highlight the importance of specific NG design elements. Disulfide bonds are highlighted as redox-sensitive cross-linkers within the NG structure as critical for drug delivery performance; they function as degradation points that enable NG degradation and subsequent drug release and anchoring points to adhere to mucin, thereby enhancing their residence time at the desired site of action. Additionally, it is confirmed that surface charges impact interactions with mucin; positively charged NGs exhibit improved interactions with mucin compared to negatively charged and neutral NGs. Overall, the findings underline the importance of redox response and surface charge in NG design for reaching efficient mucosal drug delivery.

1. Introduction

The mucus hydrogel controls the entry of bacteria, viruses, and toxins while allowing the flux of water, ions, and solutes (including nutrients).[1] This viscoelastic material forms a barrier to mucosal drug delivery, hindering the treatment of disorders that include cystic fibrosis (CF), inflammatory bowel disease (IBD), and autoimmune diseases.[2] Drugs that cannot cross mucosal barriers undergo mucociliary clearance, which can significantly reduce treatment efficacy. Utilizing small-molecule compounds like expectorants,[3] surfactants,[4] or enzyme inhibitors[5] may eliminate/disrupt the mucosal barrier and hence support the permeation of therapeutic agents; however, limitations such as a lack of therapeutic efficacy and adverse drug reactions (causing toxicity to healthy cells) have restricted treatment doses and administration frequency. Given that the mucosa protects the body against external pathogens,[6] mucosal disruption enhances the chances of infection;

J. Udabe, M. S. Orellano, M. Calderón
POLYMAT
Applied Chemistry Department
Faculty of Chemistry
University of the Basque Country UPV/EHU
Paseo Manuel de Lardizabal 3, Donostia-San Sebastián 20018, Spain
E-mail: marcelo.calderonc@ehu.eus

A. Muñoz-Juan, A. Laromaine
Institut de Ciència de Materials de Barcelona
ICMAB-CSIC
Campus UAB, Bellaterra 08193, Spain

B. Tafech, S. Hedtrich
Faculty of Pharmaceutical Sciences
University of British Columbia
2405 Wesbrook Mall, Vancouver V6T1Z3, BC, Canada

S. Hedtrich
Berlin Institute of Health @ Charité Universitätsmedizin
Lindenberger Weg 80, Berlin 13125, Germany

S. Hedtrich
Department of Infectious Diseases and Respiratory Medicine
Charité - Universitätsmedizin Berlin, corporate member of Freie
Universität Berlin and Humboldt Universität zu Berlin
Berlin, Germany

S. Hedtrich
Max-Delbrück Center for Molecular Medicine in the Helmholtz
Association (MDC)
Berlin 13125, Germany

M. Calderón
IKERBASQUE
Basque Foundation for Science
Plaza Euskadi 5, Bilbao 48009, Spain

ADVANCED
SCIENCE NEWS

www.advancedsciencenews.com

ADVANCED
FUNCTIONAL
MATERIALS

www.afm-journal.de

therefore, overcoming the mucosal barrier while preserving integrity remains imperative when addressing patient concerns.

The mucosal barrier comprises a heterogeneous layer ≈500 nm thick, predominantly composed of glycoproteins and glycolipids. This structure, known as the mucus gel, supports the entrapment and removal of pathogens.[7,8] Mucin, a glycosylated macromolecule, represents the primary secreted substance present in the mucosa.[8] Mucin entanglement forms a mucus network characterized by mesh spacing (30–500 nm) that obstructs particle diffusion through size-based separation.[9] The mucosal environment is also characterized by substantial reductive potential mediated by elevated glutathione (GSH) concentrations, a tripeptide known for its antioxidant activity.[10] High GSH concentrations raise concerns regarding drug stability, as certain pharmaceutical compounds may undergo degradation in this milieu. In disorders such as CF or asthma, spontaneous and induced sputum samples can present with even higher concentrations of reductive agents.[11] Additionally, at the cellular level, the cytosol presents higher concentrations of GSH (2–10 mmol) compared to the extracellular medium (2–20 μmol).[12]

Nanomedicine includes a variety of interdisciplinary approaches, including chemistry, pharmaceutical science, biology, and clinical medicine in order to design and synthesize biodegradable or non-biodegradable biomaterials tailored for biological, medical, and pharmaceutical uses.[13] Nanotechnology-based approaches involving biologically active and responsive materials have gained importance as promising and innovative materials in the mucosal drug delivery field.[14] Modulating nanocarrier properties (e.g., size or surface charge) represents a critical means of achieving mucoadhesiveness and increasing drug residence times.[15] The implementation of thiols and disulfide linkers within the nanocarrier structure has been linked with enhanced mucopenetration/mucoadhesion.[16] Nanogels (NGs) constitute a highly promising category of polymeric cross-linked nanocarriers, as they offer the potential for facile adjustment of their properties (e.g., size, surface charge, composition, or responsive modality) through modifications of their synthetic protocols.[17] Although GSH-responsive NGs have been widely explored for intracellular drug delivery, their ability to transport drugs across the mucosal barrier has remained, until recently, relatively unexplored;[18] the effectiveness of a controlled-release polymeric system is partially determined by its distinct physical and chemical properties, as well as its biodegradation rate.[19] Therefore, the full potential of NGs as mucosal drug delivery systems remains somewhat uncharted.

This study comprehensively investigates the interaction between thermo- and redox-responsive NGs with different elements of the mucus hydrogel. We developed NGs with differing responsivities to reductive environments and surface charges and then studied their mucosal drug delivery performance using in vitro, ex vivo, and in vivo models. We correlated their structural features with their ability to efficiently deliver our model drug, bovine serum albumin (BSA), across the mucosal barrier to provide new insight into the rational design of NGs for transmucosal drug delivery. This work highlights the vast potential of NGs in delivering biomacromolecules in challenging conditions, such as those found in the CF-affected mucus hydrogels.
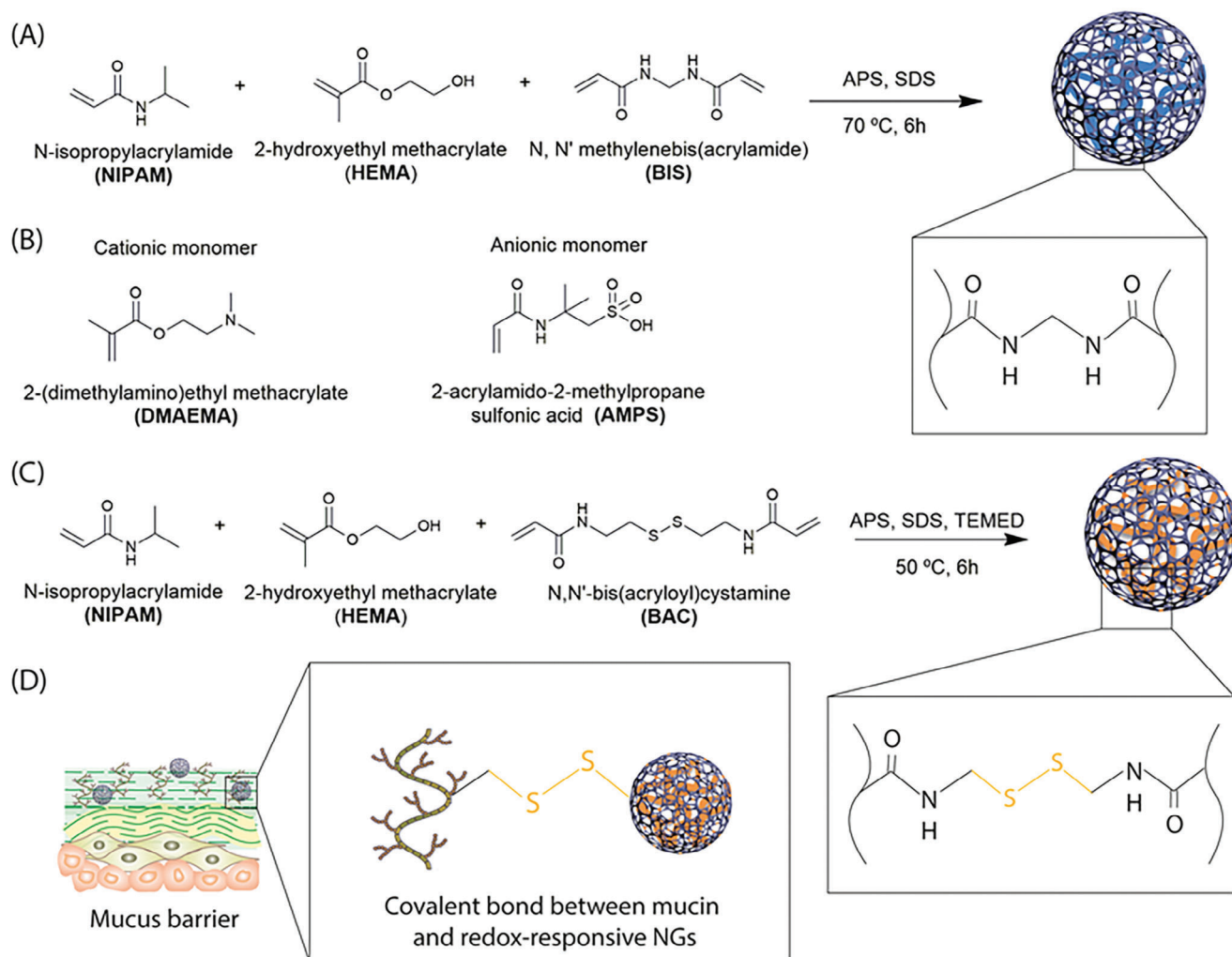
2. Results and Discussion

2.1. Synthesis and Characterization of Nanogels

We synthesized five responsive NGs by free radical precipitation polymerization to systematically investigate the influence of structural composition on mucosal drug delivery potential. As shown in **Scheme 1A–C**, N-isopropylacrylamide (NIPAM) and 2-hydroxyethyl methacrylate (HEMA) represented the main components of all NGs. Variations in the co-monomers and cross-linkers yielded NGs with different electrostatic charges or redox sensitivities. We prepared three NGs that do not respond to changes in reductive potential using N,N′-methylene bisacrylamide (BIS) as a cross-linker (Scheme 1A,B). We obtained an NG that displayed a positive charge at physiological pH after copolymerization with 2-(dimethylamino)ethyl methacrylate (DMAEMA); meanwhile, copolymerization with 2-acrylamido-2-methylpropane sulfonic acid (AMPS) yielded an NG with a negative charge. We synthesized a neutral counterpart using solely NIPAM and HEMA as co-monomers. We obtained redox-responsive NGs using N,N′-bis(acryloyl)cystamine (BAC) as a cross-linker, which contains disulfide groups that undergo cleavage under reductive conditions (Scheme 1C,D). We also prepared an NG with an equimolar composition of BIS and BAC to systematically evaluate the impact of cross-linker composition on redox-responsive behavior. The nomenclature used for all the NGs is: p(NIPAM-HEMA)(BIS), p(NIPAM-HEMA-DMAEMA)(BIS)(+), p(NIPAM-HEMA-AMPS)(BIS)(-), p(NIPAM-(S-S)-HEMA)(BIS:BAC), and p(NIPAM-(S-S)-HEMA)(BAC). In all cases, we followed synthesis by purification via dialysis and freeze drying, which yielded NGs with a white powder appearance and a high water dispersibility at an overall yield of 75–90%. We determined the chemical composition of NGs, their morphology, and the polymerization reaction kinetics by proton magnetic resonance spectroscopy (¹H-NMR), Fourier transform infrared spectroscopy (FT–IR), scanning electron microscopy (SEM), and atom force microscopy (AFM) (Figures S2–S10, Supporting Information). Except for p(NIPAM-(S-S)-HEMA)(BAC), we observed the consumption of the acrylic groups in all reactions within the first 2 h, indicating complete polymerization. The acrylic groups underwent consumption over 4 h in the case of p(NIPAM-(S-S)-HEMA)(BAC) (Figure S6, Supporting Information), suggesting the slower reactivity of BAC due to the higher hydrophobicity compared to BIS.[20,21] We measured the hydrodynamic size and ζ-potential of NGs by dynamic light scattering (DLS) and ζ-potential measurements. Table S1 (Supporting Information) shows a hydrodynamic diameter for all NGs of ≈220–250 nm, an optimum size for transmucosal drug delivery considering a mucus mesh size of 30–500 nm.[22] We also discovered a slightly negative surface potential in 10 mM phosphate-buffered saline (PBS) buffer pH 7.4 for all NGs (between −1.59 and −8.87 mV) except for p(NIPAM-HEMA-DMAEMA)(BIS)(+), which displayed a slightly positive value of +2.7 mV.

2.2. Thermo- and Redox-Responsiveness of Nanogels

We expected our synthesized NGs to display both temperature- and redox-responsive properties. NGs display a

ADVANCED
SCIENCE NEWS

www.advancedsciencenews.com

ADVANCED
FUNCTIONAL
MATERIALS

www.afm-journal.de

Scheme 1. Simplified synthetic route of each nanogel and their response. A) Synthetic scheme for non-redox responsive nanogels (NGs). B) The cationic and anionic co-monomers are used for non-redox responsive NG synthesis. C) Synthetic scheme for redox-responsive NGs. D) Representation of the covalent interaction between redox-responsive NGs and mucin. Scheme S1 (Supporting Information) provides more details of each synthetic route. APS stands for ammonium persulfate, SDS stands for sodium dodecyl sulfate, and TEMED stands for N,N,N′,N′-tetramethylethylenediamine.

thermo-responsive behavior by shrinking at temperatures above their transition temperature; meanwhile, NG redox-responsivity induces the cleavage of disulfide bonds under reductive conditions, leading to structural collapse or disassembly. We demonstrated the thermo-responsive behavior (provided by the presence of pNIPAM in the NG backbone[23]) by measuring the cloud-point temperature (T_{cp}) via turbidimetry (Table S1, Supporting Information). All NGs except for p(NIPAM-HEMA-AMPS)(BIS)(-) demonstrated the expected thermal response with a transition temperature ≈36–37 °C. A T_{cp} value of 40.8 °C for NGs bearing sulfonic acid groups (p(NIPAM-HEMA-AMPS)(BIS)(-)) provides evidence for higher hydrophilicity, highlighting the influential role of the anionic groups in behavior and phase transition.

An increased reductive environment represents a typical feature of diseased mucus-covered barriers;[11,24,25] therefore, disulfide bonds within an NG will be expected to cause structural degradation and the consequent release of an encapsu-

lated therapeutic cargo in the target diseased mucosal tissue (**Figure 1A**). We used Raman spectroscopy to determine disulfide bond cleavage under reductive conditions qualitatively; as expected, only BAC-containing NGs possessed signals corresponding to disulfide bonds (425–550 cm^{-1}, Figure 1B). Moreover, we observed the formation of free-thiols (2530–2610 cm^{-1}) when incubating redox-sensitive NGs with the reductive agent tris(2-carboxyethyl)phosphine (TCEP).

We further confirmed the structural collapse of redox-responsive NGs with SEM, gel permeation chromatography (GPC) (Figures 1C,D, respectively), and DLS (Figure S11, Supporting Information). We incubated NGs with varying GSH concentrations for varying incubation times. Figures 1C,D demonstrate that p(NIPAM-(S-S)-HEMA)(BIS:BAC) became fragmented into small pieces within 1 week of incubation under reductive conditions. We verified this overall tendency thanks to the increased retention times and distributions observed in GPC analyses and the size decrease observed in SEM images
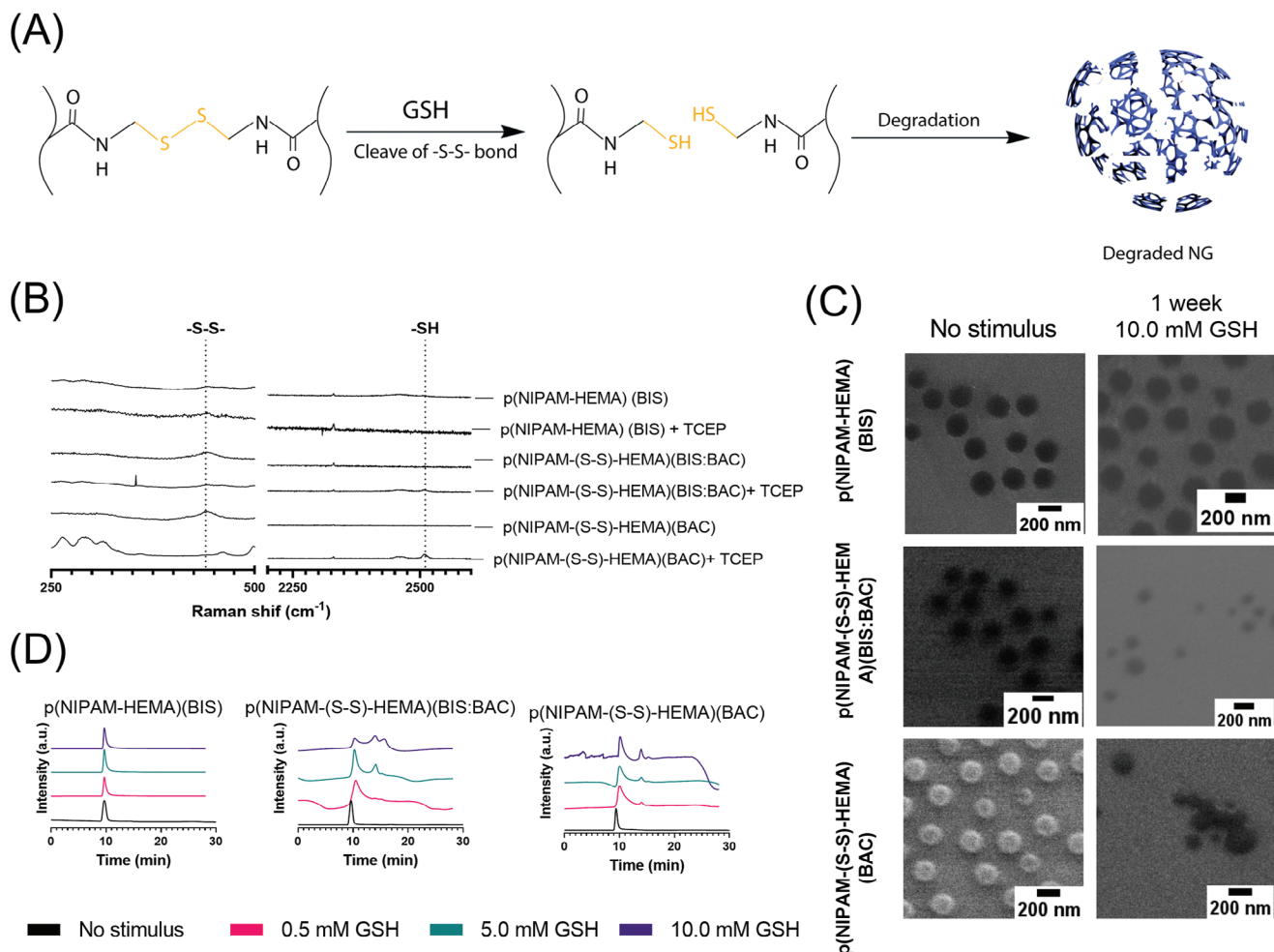
**ADVANCED
SCIENCE NEWS**

www.advancedsciencenews.com

**ADVANCED
FUNCTIONAL
MATERIALS**

www.afm-journal.de

Figure 1. Degradation behavior of redox-responsive nanogels. A) Schematic illustration of the degradation of redox-responsive nanogels (NGs). B) Raman spectroscopy with/without 10 mM tris(2-carboxyethyl)phosphine (TCEP) treatment. C) Scanning electron microscopy (SEM) images reveal the structural evolution of redox-responsive NGs in the absence (labeled as no stimulus) and the presence of 10 mM glutathione (GSH) for 1 week. D) Gel permeation chromatography (GPC) profiles reveal retention time evolution in the absence or presence of differing GSH concentrations at several time points. Figures S12,S13 (Supporting Information) present detailed data for RAMAN and GPC of all NGs. The information on the mean diameter of the diameter of nanogels obtained from TEM can be found in Table S6 (Supporting Information).

(Table S6, Supporting Information). Similarly, we noted a size reduction accompanied by an increase in the polydispersity index (PDI) by DLS analysis for BAC-containing NGs when incubated with GSH (Figure S11, Supporting Information), which might facilitate the in vivo clearance of redox-responsive NGs;[26,27] however, subsequent analyses by DLS and SEM after 1 week revealed a noteworthy increase in both the size and PDI of p(NIPAM-(S-S)-HEMA)(BAC), indicating probable aggregation. In comparison, non-redox-responsive NGs incubated with GSH maintained similar sizes and morphologies for all concentrations at all measured times.

2.3. Studies of Nanogel-Mucin/Mucus Interactions

As a first attempt to analyze NG-mucus interactions, we quantified the interaction strength by rheology since the physical and chemical bonds of the molecules are transformed in mechanical

energy in the interaction and change the viscosity. We recorded changes in viscosity after mixing solutions of NGs and mucin and determined the interaction force (**Figure 2A**); overall, we obtained mean values ranging between 7–23 dyne cm^{-2}. We observed a statistically significant 2–3 fold increase in the mucoadhesive force for p(NIPAM-(S-S)-HEMA)(BAC) compared to the remaining NGs, which could be attributed to the capacity of this NG to form covalent linkages with the free thiols of mucin. The adhesive force of 23 ± 7 dyne cm^{-2} obtained for p(NIPAM-(S-S)-HEMA)(BAC) compares well to values previously obtained for moderately adhesive formulations.[28]

Next, we analyzed the potential of NGs to penetrate through healthy mucus, which contains a relatively low concentration of glutathione compared to unhealthy mucus,[10] using a transwell diffusion apparatus with mucus extracted from the calf's small intestine to quantify NG penetration over time. Figure 2B demonstrates that all NGs crossed the modeled mucosa over 24 h, proving that these NGs can permeate mucus barriers. While we
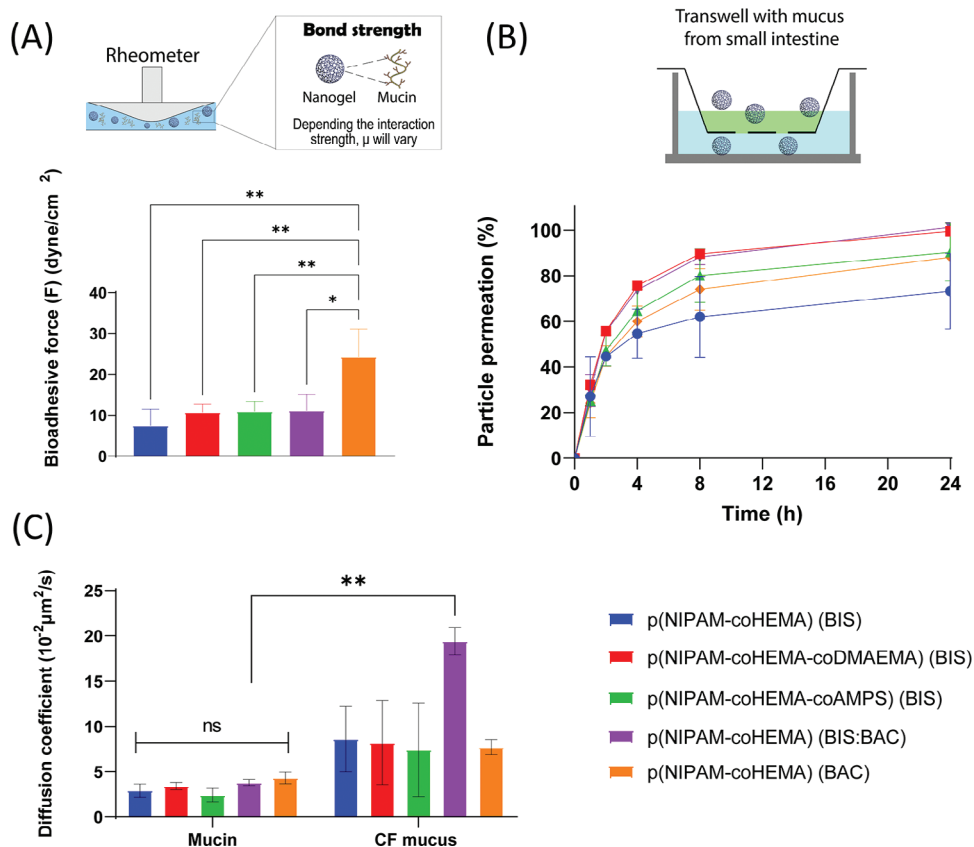
Figure 2. Nanogel-mucin/mucus interactions. A) Bioadhesive force between nanogels (NGs) and mucin measured by viscosity (μ) on a rheometer. ($n = 3$). B) Particle permeation study in mucus extracted from porcine intestine ($n = 3$). C) Median diffusion mucus/mucin mobility assay; an average of 339 particles were analyzed per NG. Data represented as mean ± standard deviation. Statistical analysis processed by two-way ANOVA with multiple comparisons test, $^{***}p < 0.001$, $^{**}p < 0.01$, $^{*}p < 0.05$).

did not observe any statistically significant differences in mucus-penetrating behavior between the NGs under these experimental conditions (37 °C), a trend was noted. All NGs exhibited transmucosal penetration within the first 8 h before reaching a subsequent plateau. We hypothesize that initially, the NGs that have not interacted with the mucosal barrier pass through it. As time progresses, interactions are formed, thereby reducing the permeation kinetics and leading to a plateau.

To further analyze the potential of NGs for transmucosal drug delivery, we studied their mobility in normal mucus hydrogels and mucus derived from CF patients (CF mucus) by multiple particle tracking by fluorescence microscopy. As extensively described in the literature, mucosa derived from diseased conditions, specifically mucosa extracted from patients with CF, contains elevated concentrations of GSH;[11] thus, promoting responsiveness in the redox-responsive NGs. As shown in Figure 2C, we observed the decreased mobility of NGs in mucin with increased BAC composition, perhaps due to their increased capacity to form disulfide bonds with mucin. We also observed that the negatively charged NG (p(NIPAM-HEMA-AMPS)(BIS)(-)) displayed lower mobility compared to a positively charged counterpart, likely due to the repulsive forces induced by the negatively charged mucin.[29,30] We observed a similar trend in the

case of NGs incubated with CF mucus; however, p(NIPAM-(S-S)-HEMA)(BIS:BAC) displayed a significant increase in mobility compared to the remaining NGs, most likely due to the high GSH concentration found in the CF mucus. Under these conditions, both BAC-containing NGs would suffer degradation and a consequent decrease in size, which increases their ability to penetrate through the mucus mesh; however, the elevated thiol/disulfide exchange capacity of p(NIPAM-(S-S)-HEMA)(BAC) with components of the mucosal barrier may result in decreased mobility.

2.4. Temperature- and Redox-Induced Drug Release from NGs

Next, we conducted release studies to demonstrate the capacity of NGs for controlled drug delivery/release under healthy and diseased mucus conditions. We selected bovine serum albumin labeled with fluorescein isothiocyanate (BSA-FITC) as a model protein for encapsulation, storage, and drug release studies. Overall, we obtained high encapsulation efficiency (>90%) and loading capacity (≈65 wt.%) for all NGs (Table S3, Supporting Information); moreover, all NGs efficiently retained BSA-FITC for at least a month under refrigerated conditions, with the release by diffusion observed at below 5%. All NGs released their cargo when incubated at a temperature above their T_{CP} due to NG

ADVANCED
SCIENCE NEWS

www.advancedsciencenews.com

ADVANCED
FUNCTIONAL
MATERIALS

www.afm-journal.de

shrinkage and the expulsion of their contents. The p(NIPAM-HEMA-AMPS)(BIS)(-) NG displayed slower release kinetics than the remaining NGs, perhaps due to the higher T_{CP} value when compared with other NGs. Based on the structure of redox-responsive NGs, we assumed that redox-response-mediated drug release exhibited rapid but sustained release kinetics, which describes the combinational effects of the erosion of the reduced polymeric cross-linker and BSA-FITC dissolution and diffusion. Under reductive conditions, we observed that release predominantly occurred in BAC-containing NGs, while the remaining NGs exhibited low release ($\leq$10%); furthermore, we observed a trend for a more rapid release of a greater extent of BSA-FITC at higher GSH concentrations. As observed in **Figures 3A** and S13 (Supporting Information), BAC-containing NGs retained BSA-FITC (release below 10%) without a reductive stimulus; however, release from redox-responsive NGs accelerated when incubating NGs with 5 or 10 mM GSH. The release profiles for p(NIPAM-(S-S)-HEMA)(BIS:BAC) and p(NIPAM-(S-S)-HEMA)(BAC) incubated with 5 mM GSH fitted the Higuchi and Baker-and-Lonsdale models, respectively, which can elucidate the drug release mechanism (the Fickian diffusion specifically) from an insoluble matrix.[31] These findings indicate that the cross-linkers of redox-responsive NGs partially degrade under reductive conditions with GSH concentrations $\approx$5 mM, thereby decreasing the cross-linking density and allowing cargo diffusion. When incubated with 10 mM GSH, BSA-FITC release presents a rapid zero-order release profile (Table S4, Supporting Information). A rapid and constant release rate characterizes this type of release,[32,33] which provides evidence for the rapid degradation of NGs followed by a burst release of BSA-FITC trapped in the polymeric network. Finally, we observed that p(NIPAM-(S-S)-HEMA)(BAC) exhibited higher release compared to p(NIPAM-(S-S)-HEMA)(BIS:BAC), which suggests that increasing the concentration of the redox-responsive cross-linker enhances stimuli responsiveness, thereby increasing the release capacity.

We also studied the penetration of NG-encapsulated BSA-FITC in excised bovine small intestine; we quantified green fluorescence intensity using ImageJ software to determine the differential BSA-FITC penetration provided by NGs (Figure 3B). The quantified area corresponds to the top of the tissue up to the muscle (dotted line). Remarkably, p(NIPAM-HEMA-DMAEMA)(BIS)(+) exhibited significantly higher BSA-FITC penetration than the remaining NGs. The significantly lower penetration of the protein loaded into the negatively charged p(NIPAM-HEMA-AMPS)(BIS)(-) suggests that the surface charge of the NGs strongly influences the penetration of the cargo across this mucosal barrier. Figure 3C displays representative cross-tissue sections of the small intestine incubated with the NGs used for fluorescence quantification, which reveals the green fluorescence from BSA-FITC indicative of mucosal penetration. We observed that p(NIPAM-HEMA-DMAEMA)(BIS)(+) NGs showed higher green fluorescence compared to other samples, indicating that these NGs promote higher penetration of the cargo. The higher BSA-FITC penetration observed for p(NIPAM-HEMA-DMAEMA)(BIS)(+) NGs could be explained by the positive surface charge under physiological conditions, which can interact with the negative moieties of mucin via electrostatic interactions. Thus, our results show that a higher NG mucoadhesion level correlates with a higher penetrated protein, which agrees with previous reports that attributed the enhanced diffusion of loaded drugs through the mucosal barrier to the nanocarrier's mucoadhesion properties.[34] Interestingly, the fluorescence images of Figure 3C illustrate that BSA-FITC can go deeper across this mucosal barrier when encapsulated within BAC-bearing NGs, although the overall fluorescence quantification of BSA-FITC (Figure 3B) did not show significant differences with p(NIPAM-HEMA)(BIS) and p(NIPAM-HEMA-AMPS)(BIS)(-) NGs. This observation also suggests that the interaction of NGs with the mucosal barrier plays an important role in cargo diffusion. We could attribute the deeper penetration depth observed for BAC-bearing NGs in imaging to the disulfide bonds within the mucus-interacting structure, which facilitates enhanced cargo diffusion through the mucosal barrier.

To further analyze the protein delivery capacity of NGs in the reductive environment of the diseased mucosa,[11] we studied the mucosal penetration of BSA-FITC loaded in Rhodamine B-labeled NGs (synthesized as shown in Scheme S2, Supporting Information) by epifluorescence microscopy. For this experiment, we prepared a thin mucus layer using isolated mucus from small intestine tissue in a glass chamber. We placed protein-loaded NGs on the mucosal surface and incubated for 2 h under two conditions: 37 °C at 0 mM GSH and 10 mM GSH. We then quantified the green and red fluorescence corresponding to the penetrated protein and penetrated NGs, respectively, at different z depths. Figure S15 (Supporting Information) displays a z-axis profile plotted with ImageJ software, representing the mean fluorescence intensity of green and red channels of each xy plane at different depths. The increased fluorescence intensity as depth increases indicates higher BSA-FITC/NGs penetration. The quantification of FITC and Rhodamine-B channels allows us to compare how is the relative diffusion of the encapsulated protein and the NGs through the mucosal layer. Figure S15 (Supporting Information) demonstrates increased green fluorescence intensity as depth increases for all formulations in the non-reductive condition (0 mM GSH), indicating that BSA-FITC penetrated across the mucosal layer when encapsulated by all NGs. This behavior agrees with the finding shown in Figures 3B,C. Regarding the penetration profile of NGs, treatment with p(NIPAM-HEMA-DMAEMA)(BIS)(+), p(NIPAM-(S-S)-HEMA)(BIS:BAC), and p(NIPAM-(S-S)-HEMA)(BAC) showed a decrease in red fluorescence intensity as depth increases, which indicates that NGs mostly remain near the mucosal surface. This trend evidences that these NGs display higher adhesion to the mucosal layer, meanwhile enabling higher BSA-FITC penetration. Interestingly, p(NIPAM-HEMA)(BIS) and p(NIPAM-HEMA-AMPS)(BIS)(-) showed the opposite trend—increased red intensity as depth increases—indicating that NGs diffuse across the mucosal layer together with the loaded protein.

When comparing the behavior of formulations under reductive conditions (10 mM GSH), we found similar tendencies for protein penetration through the mucosa to the non-reductive condition. The most relevant differences include the drastically increased red fluorescence profile for p(NIPAM-(S-S)-HEMA)(BIS:BAC) and p(NIPAM-(S-S)-HEMA)(BAC), as depth increased. NG degradation under a reductive environment can explain the higher penetration observed.[18] Overall, this diffusion assessment confirmed the higher adhesion of p(NIPAM-HEMA-DMAEMA)(BIS)(+), p(NIPAM-(S-S)-HEMA)(BIS:BAC),
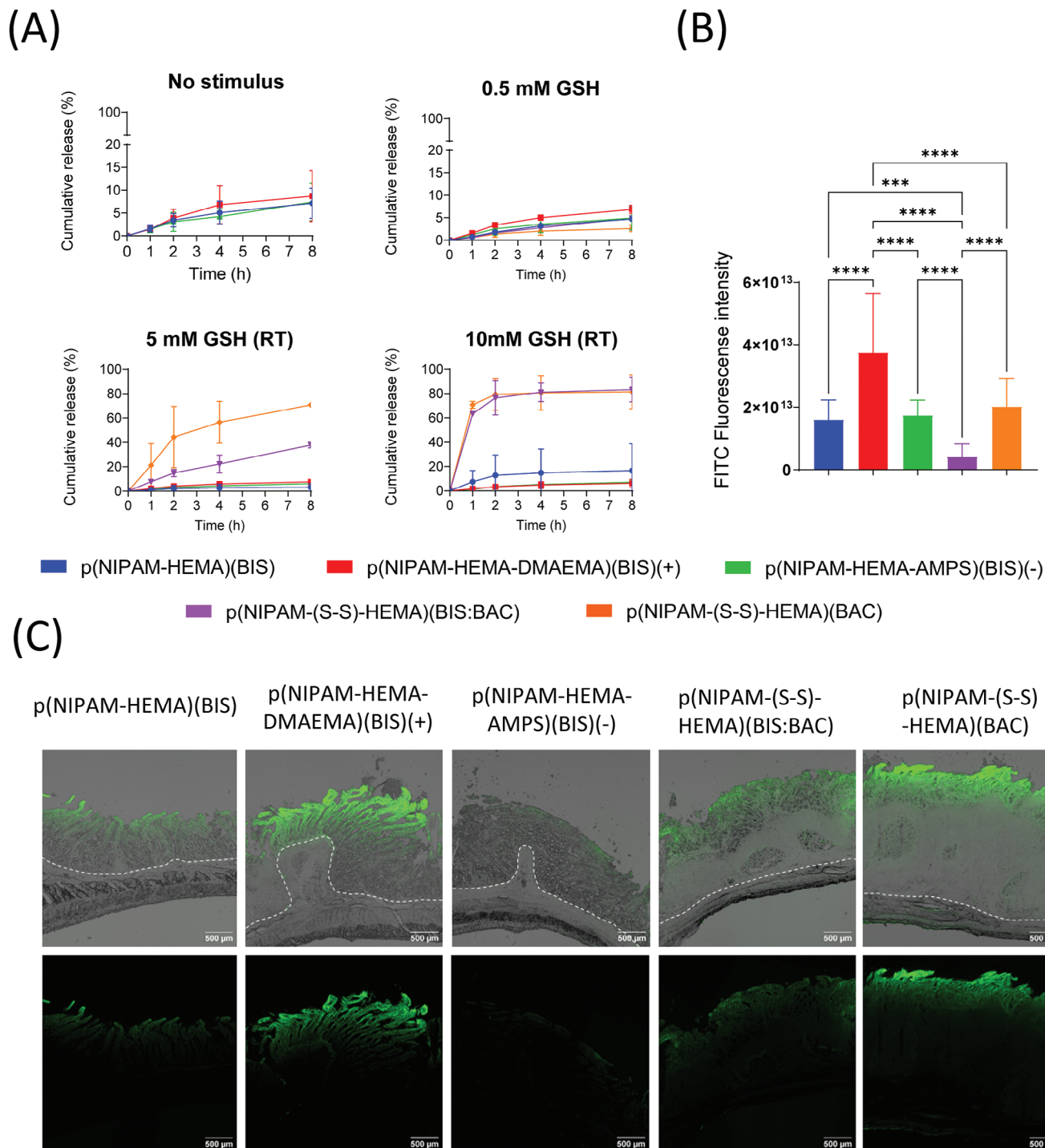
Figure 3. Drug release studies and mucus penetration of a model encapsulated protein in an *ex vivo* small intestine model. A) I*n vitro* cumulative drug release of bovine serum albumin labeled with fluorescein isothiocyanate (BSA-FITC) from nanogels (NGs) exposed to varying concentrations of glutathione (GSH) for varying times. More information on the release at 37 °C in 0, 0.5, 5.0, and 10 м GSH of the NGs in Figure S15 (Supporting Information). B) Green fluorescence intensity quantification of penetrating BSA-FITC after 2 h incubation at 37 °C. At least fifteen sections were analyzed. Statistical analysis processed by two-way ANOVA with Bonferroni's multiple comparisons test ($^{****}p < 0.0001$, $^{***}p < 0.001$, $^{**}p < 0.01$, $^{*}p < 0.05$). C) Fluorescence imaging of small intestine sections after the 2 h incubation at 37 °C (Scale bar = 500 μm).
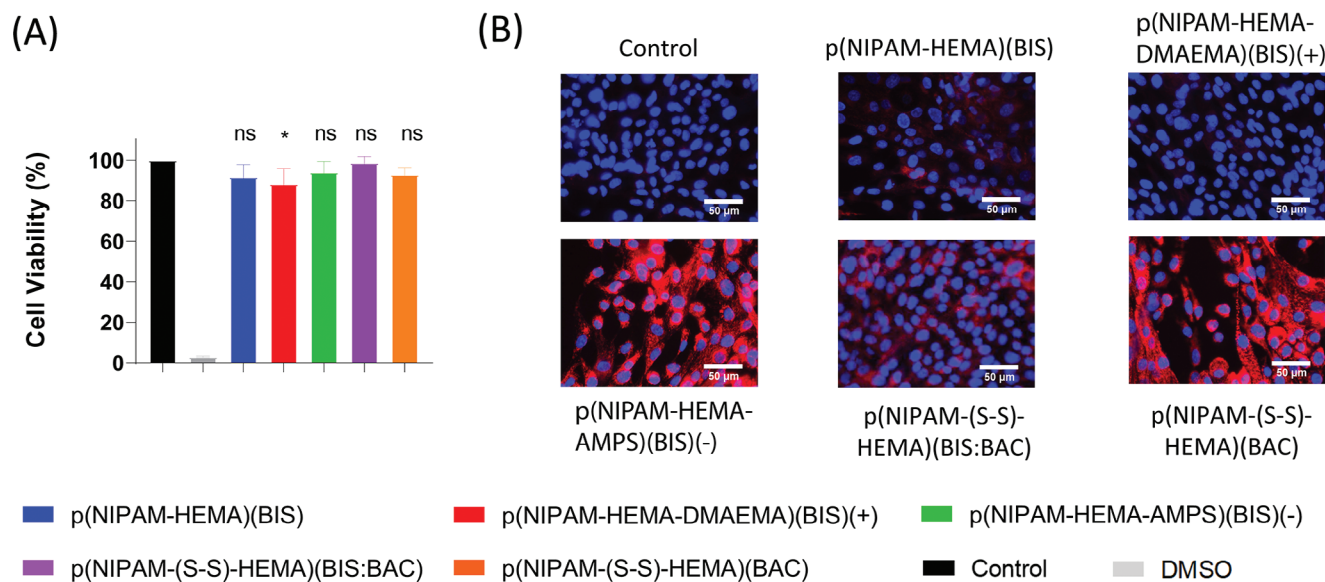
Figure 4. Nanogel evaluation in cells. A) Cell viability studies in bronchial epithelial (HBE) cells treated with nanogels (NGs) at 1 mg mL^{-1} concentration over 24 h; HBE cells were incubated in growth media as a untreated (healthy) control and in 10% dimethyl sulfoxide (DMSO) solution as a cytotoxic control. B) Cell uptake studies in HBE cells using Rhodamine B-labeled NGs. All data represented as mean ± standard deviation; $n = 3$. GraphPad Prism v9 was used for statistical analysis and graphical representation ($^*p < 0.05$, ns; no statistical difference).

and p(NIPAM-(S-S)-HEMA)(BAC) and highlights the relevance of disulfide bonds in NG structure concerning enhancing NG/cargo penetration through the mucosal barrier in diseased conditions.

2.5. Assessment of Nanogel Cellular Uptake and Cytocompatibility

To further assess the therapeutic potential of NGs, we evaluated their interaction, cell viability, and NG uptake with mucus-producing primary human bronchial epithelial cells (HBE). We incubated cells with 1 mg mL^{-1} solutions of respective NGs (a high concentration in the biomedical field[35]) for 24 h. As shown in **Figure 4A**, the cell viability observed after incubation of most NGs failed to display significant differences compared to the control (untreated control sample). Despite the significant decrease in cell viability observed for the positively charged p(NIPAM-HEMA-DMAEMA)(BIS)(+) compared to the control ($p < 0.05$), cell viability remained at 85–90% even at high concentrations. Figure 4B demonstrates that BAC-containing NGs and p(NIPAM-HEMA-AMPS)(BIS)(-) NGs displayed the highest uptake by HBE cells after 4 h incubation. A previous study reported that the thiol-disulfide exchange pathway improves cell membrane penetration;[36] thus, we may be able to exploit dynamic interactions between disulfide-containing NGs and disulfide/thiol bonds in transmembrane proteins to enhance cell internalization. Disulfide group-containing NGs can undergo endosomal escape,[37] while non-redox-responsive NGs remain trapped. Hence, we hypothesize that the increased availability of disulfide groups on the surface of p(NIPAM-(S-S)-HEMA)(BAC) resulted in enhanced cellular uptake and improved endosomal escape. Surprisingly, HBE cells took up p(NIPAM-HEMA-AMPS)(BIS)(-) to a greater extent than p(NIPAM-HEMA-DMAEMA)(BIS)(+).

Positively-charged nanocarriers become internalized to a greater extent than neutral or negatively charged counterparts;[38–42] however, the role of nanoparticle surface charge on cellular uptake remains controversial. Lunov et al. studied cell uptake with both anionic and cationic nanoparticles,[43] revealing that macrophages preferred to uptake anionic nanoparticles through endocytosis, whereas monocytes favored cationic nanoparticles. Hence, this study may have encountered varying mechanisms of cellular uptake, with p(NIPAM-HEMA-AMPS)(BIS)(-) uptake more efficient than that observed for p(NIPAM-HEMA-DMAEMA)(BIS)(+).

2.6. A Comprehensive Evaluation of Nanogels in the Model Animal *C. elegans*

Next, we evaluated the interaction of NGs with the intestinal barrier using the invertebrate model *Caenorhabditis elegans* (*C. elegans*). This 1 mm long nematode shares 60% genetic homology with humans and has been broadly applied in nanomaterial testing.[44] The resemblance between *C. elegans* and the human intestine is particularly interesting for evaluating NGs. The *C. elegans* intestine comprises twenty polarized cells, with microvilli and glycocalyx—a protein-rich layer whose composition remains not fully characterized but it contains heparin sulfate and dermatan sulfate[45] in the apical membrane (**Figure 5A**).[46] This complex barrier protects intestinal cells against mechanical damage and pathogens while acting as a scaffold for enzymes and a filter for the lumen's content.

We exposed synchronized L4 worms to NGs and evaluated the survival rate and alterations to body size after 24 h (ultrapure water acted as a negative control, and 5% DMSO acted as a positive control for toxicity). p(NIPAM-HEMA-DMAEMA)(BIS)(+) exposure prompted a significant reduction in the survival rate
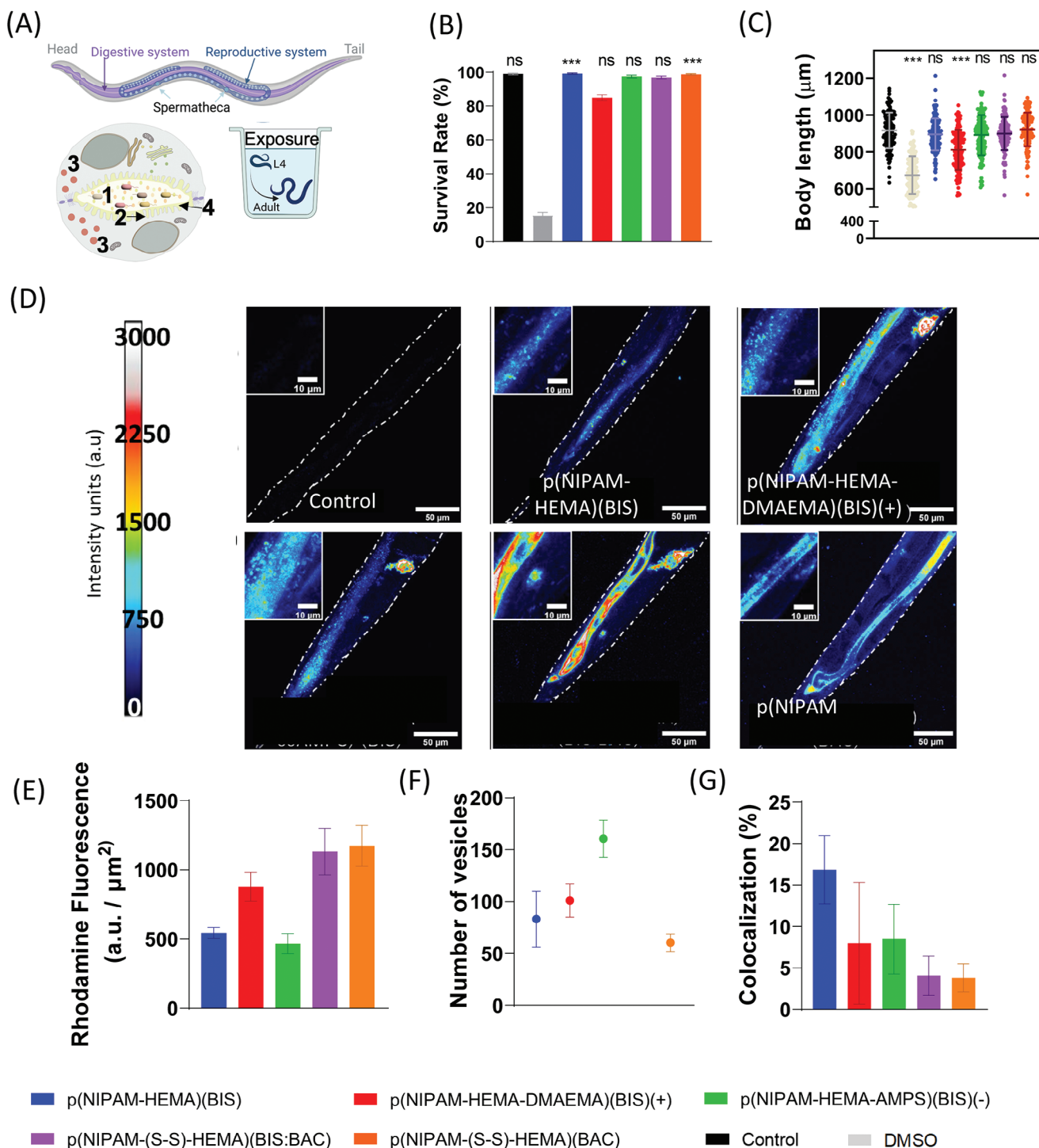
Figure 5. Nanogel evaluations in a *C. elegans* model. A) The anatomical structure of *C. elegans*, with particular focus on the intestinal tract – 1) lumen; 2) microvilli with actin bundles; 3) nucleus; 4) glycocalyx – and the exposure conditions. B,C) Effect of nanogel (NGs) on B) survival rate (mean ± SEM, as compared to purified water (Control)) and C) body length (mean ± SD, as compared to purified water (Control)). DMSO was used as a positive control for toxicity. D) 2D summation of confocal Image Z-stacks of the red channel analyzed with Royal Lookup Table of control and NG-treated worms. Images were adjusted to maintain the same intensity range (represented with a color legend with 0 to 3000 intensity values on the left). The inset at the top left of each image represents a zoom image of the intestine used to visualize vesicles. E) Nanogel concentration in worms is represented by the mean red fluorescence intensity normalized to the total area of the image. F) Number of BSA-FITC vesicles visualized that crossed the intestinal barrier in the tail region for each NG-treated group n = 5. G) Colocalizing green and red fluorescence to assess BSA-FITC release from Rhodamine B-labeled NGs. All data represented as mean ± standard deviation; *n* > 3. *C. elegans* characterization employed the Kruskal test with Dunn's post-correction, as samples did not follow a parametric distribution. GraphPad Prism v9 used for statistical analysis and graphical representation, *** *p* < 0.001, ns no statistical difference.

**ADVANCED
SCIENCE NEWS**

www.advancedsciencenews.com

**ADVANCED
FUNCTIONAL
MATERIALS**

www.afm-journal.de

to 85 ± 2% (mean ± SEM, $p < 0.001$[***]) compared to the negative control, all remaining NGs supported a survival rate of over 95% (Figure 5B). Interestingly, we found that p(NIPAM-HEMA-DMAEMA)(BIS)(+)-treated L4 worms (initially ≈650 µm long) were shorter than the negative control and other NG-treated worms ($p < 0.001$[***]) (Figure 5C). Worms exposed to 5% DMSO died without developing, displaying an average size of 674 ± 103 µm. Interestingly, p(NIPAM-HEMA-DMAEMA)(BIS)(+)-treated worms grew to 811 ± 109 µm ($p < 0.001$[***] to control and DMSO-treated worms), indicating that the decrease of the survival rate was not as substantial as DMSO and allowed the worms to develop further although not to the same size as control worms (917 ± 97 µm long) (Figure 5B). These results indicate good NG biocompatibility of total negative surface charge and detrimental impact of the positively-charged p(NIPAM-HEMA-DMAEMA)(BIS)(+) (2.7 ± 0.5 mV in 10 mм PBS buffer pH 7.4). Studies have suggested that a positive surface charge could cause toxicity in *C. elegans*.[47] Furthermore, these findings align with the outcomes of the in vitro cell viability assays performed in HBE cells.

Next, we studied the biodistribution of NGs throughout the intestinal tract using Rhodamine B-labeled NGs encapsulating BSA-FITC (Figures 5D,E). The optical microscope imaging revealed the presence of NGs in the intestinal lumen (Figure S16, Supporting Information), and confocal microscopy allowed for a more detailed analysis of the intestinal permeation of each NG. We focused on the tail region (Figure S17, Supporting Information), given that this segment encompasses the final part of the digestive tract. The red fluoresced due to the Rhodamine B was assigned to the NGs, and it was detected inside and outside the intestinal lumen (forming vesicles), and a strong signal in the spermatheca (Figure 5B), indicating the permeation of the intestinal barrier for all NGs. To note, is the detection of vesicles outside the intestinal lumen, containing NGs, confirming the translocation of NGs. We measured the red fluorescence intensity and normalized it by area, revealing that worms treated with p(NIPAM-(S-S)-HEMA)(BIS:BAC) and p(NIPAM-(S-S)-HEMA)(BAC) tended to possess a higher mean red fluorescence intensity than other NGs (Figure 5E), although differences were not significant. Furthermore, p(NIPAM-HEMA-DMAEMA)(BIS)(+) had a higher red fluorescence intensity than p(NIPAM-HEMA)(BIS) and p(NIPAM-HEMA-AMPS)(BIS)(-), suggesting again that positive charges alter any organismal interactions (Figure 5E). We also quantified fluorescence inside the intestine and the amount of NGs that passed through the intestinal barrier (Figure S18, Supporting Information), finding that p(NIPAM-HEMA-DMAEMA)(BIS)(+) treatment induced a higher fluorescence intensity than other NGs outside the intestinal lumen, although differences were not statistically significant. Reports have suggested that positive charges may disrupt the attractive forces existing between a nanomaterial and *C. elegans*,[45] thus promoting the permeation of the intestinal barrier; meanwhile, other studies have indicated that positively charged nanomaterials could interact with the proteins, polysaccharides, or bacteria in the *C. elegans* media, rendering their nutrients inaccessible.[48]

To measure the translocation of the intestinal barrier by NGs, we employed high-resolution confocal microscopy to compute the internal intestinal vesicles with NGs secreted from the intestinal lumen (Figure 5F) by ImageJ Fiji 3D Object counter.[49]

This analysis differentiates the intestinal lumen region of worms from the intestinal cells thanks to the significant green intensity found in the lumen. However, the quantification of vesicles in response to p(NIPAM-(S-S)-HEMA)(BIS:BAC) exposure was unfeasible due to the inability to discern the intestinal lumen in this condition. Among the remaining NGs, we computed the highest vesicle count for p(NIPAM-HEMA-AMPS)(BIS)(-) (Figure 5F), with no substantial variance noted in area or volume (Figure S19, Supporting Information). These findings indicate that *C. elegans* digested comparable quantities of NGs, but in some instances, a higher degree of internalization occurred within vesicles.

We then sought to monitor the colocalization of the BSA-FITC signal with the red signal of Rhodamine B-labeled NGs to study the release of the cargo molecule throughout *C. elegans*, although with specific emphasis placed on the tail (as before) (Figure 5G). A colocalization value of 0% suggests the complete release of the BSA-FITC from the Rhodamine B-labeled NGs, while 100% indicates that BSA-FITC remains encapsulated in NGs. Here, we observed colocalization values lower than 25% for all NGs, indicating the release of the cargo. While we found no significant differences between NGs, p(NIPAM-(S-S)-HEMA)(BAC) and p(NIPAM-(S-S)-HEMA)(BIS:BAC) provided a somewhat lower colocalization percentage, suggesting the potential relevance of BAC to enhance the release of the encapsulated BSA-FITC.

Finally, we evaluated the possible retention of NGs in the intestinal tract of *C. elegans* after 5 h of exposure, and then we transferred worms to fresh plates with food. We then recollected worms and anesthetized them to support imaging using a confocal microscope (Figure S20, Supporting Information). We did not detect red fluorescence in worms exposed to any NG except for p(NIPAM-HEMA-DMAEMA)(BIS)(+), presenting a low-level fluorescence intensity in the pharynx. We still observed BSA-FITC granules after this time, especially in worms exposed to p(NIPAM-HEMA)(BIS), p(NIPAM-HEMA-DMAEMA)(BIS)(+), p(NIPAM-HEMA-AMPS)(BIS)(-), which may indicate (as observed in in vitro characterizations) that BAC-containing NGs undergo degradation, making them more easily eliminated, and hence undetectable.

3. Conclusion

The present study describes the preparation of stable, spherical NGs of varying composition with hydrodynamic diameters of ≈220 nm. Synthesized NGs displayed temperature-dependent swelling/shrinking properties; two presented redox-responsive behaviors. The presence of BAC as a cross-linking agent within the NG structure imparted the capacity for partial degradation in reductive environments; overall, we observed more prominent degradation with increased exposure time/reductive agent concentrations. Rheological characterization confirmed greater bond strength between the mucin and disulfide groups; this covalent union represents a promising strategy to selectively enhance interactions between NGs and mucosa for improved targeted drug delivery. The mucus-modified transwell technique demonstrated efficient transmucosal permeation of the NGs under the studied conditions.

We demonstrated that NGs efficiently encapsulated BSA-FITC (a model protein) with almost no release (<5%) under

**ADVANCED
SCIENCE NEWS**

www.advancedsciencenews.com

**ADVANCED
FUNCTIONAL
MATERIALS**

www.afm-journal.de

refrigerated storage conditions (4 °C) over a month. Release studies demonstrated that all NGs released their cargo at physiological temperatures; moreover, higher reductive agent concentrations or disulfide-containing cross-linker percentages prompted more rapid and more significant cargo release from redox-responsive NGs. Penetration studies using an *ex vivo* small intestine model revealed that positively charged NGs robustly promoted cargo penetration compared to negatively charged/neutral NGs. Also, NGs bearing redox-sensitive bonds enhanced BSA-FITC diffusion depth through mucosal barriers. The penetration study of BSA-FITC encapsulated into labeled NGs through a mucosal layer revealed that positively charged NGs and BAC-bearing NGs exhibit higher adhesion to the mucosal layer and allow higher protein penetration.

Cell studies suggested that NGs generally lacked cytotoxicity when evaluated in HBE cells at 1 mg mL^{-1} concentrations; furthermore, as several previous studies had suggested, we found that BAC-containing NGs underwent enhanced cellular uptake. Subsequent evaluation in *C. elegans* explored the interaction of NGs with an entire living organism for the first time. *C. elegans* experiments set the first evidence of NGs' biocompatibility and intestinal barrier translocation in an alive organism. However, due to *C. elegans* limitations, further evaluation in mammal models would be required for their use in nanomedicine. Despite the evolutionary distance from humans, the *C. elegans* intestine shares similarities with humans and supports the evaluation of novel nanomaterials. These analyses confirmed the biocompatibility of NGs, although we did observe some adverse effects of p(NIPAM-HEMA-DMAEMA)(BIS)(+) on survival and development. *C. elegans* internalized all NGs, but those containing BAC become more concentrated, possibly due to greater mucoadhesion. In this case, NGs uptake occurred via endocytosis, and BAC-containing NGs possessed a better BSA-FITC release profile.

Together, these results describe a promising approach to developing NGs with temperature- and/or redox-responsive behavior and significantly contribute to exploring the interaction between NGs and elements of the mucosal barrier. This knowledge provides a foundation for developing a systematic and rational design approach for NGs tailored to deliver therapeutics in the context of mucosal barrier-related diseases effectively.

4. Experimental Section

Materials: 4-Dimethylaminopyridine 98% (DMAP) was purchased from Acros Organics; N,N′-Bis(acryloyl)cystamine 98% (BAC) from Alfa Aesar; ammonium persulfate 98% (APS), deuterium oxide (D2O) ((deuteration degree min. 99.95% for NMR spectroscopy), hydroquinone 98% (HQ), N,N-dimethylformamide (anhydrous, 99.8%) (DMF), rose Bengal 85% (RB) and sodium acetate ≥99% (NaAc) from Scharlau; 2-(Dimethylamino)ethyl methacrylate 98% (DMAEMA), 2-Hydroxyethyl methacrylate 97% (HEMA), albumin-fluorescein isothiocyanate conjugate (Protein bovine) (BSA-FITC), deuterated dimethyl sulfoxide (deuteration degree min. 99.95% for NMR spectroscopy) (DMSO-d6), glutathione (Pharmaceutical Secondary Standard; Certified Reference Material) (GSH), N-Isopropylacrylamide ≥99% (NIPAM), N, N′ Methylenebis(acrylamide) 99% (BIS), N,N,N′,N′-Tetramethylethane-1,2-diamine 97% (TEMED), mucin from porcine stomach (Type II), sodium dodecyl sulfate ≥99.0% (SDS) and tris(2-carboxyethyl)phosphine hydrochloride ≥98% (TCEP) from Sigma–Aldrich; Ready-Cal-Kit PEO/PEG from Testa Analytical Solutions; 1,4-Dithiothreitol ≥98%,

(DTT), 2-Acrylamido-2-methyl-1-propanesulfonic 97% (AMPS), N,N′-diciclohexilcarbodiimida 99% (DCC), phosphate-buffered saline (PBS) and Rhodamine B f 98% from ThermoFischer. 10 kDa molecular weight cut-off (MWCO) Pierce Protein Concentrators PES columns as well as Hoechst 33342. Solutions were obtained from Thermo Fisher Scientific (Burlington, ON, Canada). CF mucus collection was facilitated by Clinicians from Providence Health Care (Vancouver, BC, Canada) from CF patients at Sant Paul's Hospital, Vancouver, BC, Canada (Ethics approval number: H20-03198). PneumaCult-Ex Plus Medium was from STEMCELL (Vancouver, BC, Canada). Primary human bronchial epithelial (HBE) cells were purchased from the Cystic Fibrosis Translational Research Centre at McGill University (Montreal, QC, Canada) and Epithelix (Geneva, Switzerland). HBEs were maintained in PneumaCult-Ex Plus Media. HBEs were maintained at 37 °C in a humidified atmosphere of 5% CO$_2$.

It was determined through an Ellman assay that both the commercial mucin and the healthy mucosa extracted from the porcine stomach did not contain GSH.

Preparation of Temperature- and/or Redox-Responsive NGs: NGs were synthesized by precipitation polymerization (exact quantities can be found in Table S6, Supporting Information). The experiments were carried out in a 50 mL three-necked round-bottomed flask, equipped with a mechanical stirrer, reflux condenser, thermometer, and gas inlet. To adjust the glass transition of the final polymer to a physiological temperature, a mol ratio of ≈97:3 NIPAM and HEMA was used. Typically, the monomers and co-monomers (≈1 mmol), cross-linker (0.05 mmol in total), and SDS (0.02 mmol) was dissolved in 9.5 mL ultrapure water and purged with argon for 30 min. In the case of using the DMAEMA monomer, it is reacted at a pH of 9, adjusted with 0.1 M HCl solution, and the DMAEMA monomer is added 1 h after adding the initiator. In order to avoid the possible electrostatic reaction between the monomer and the initiator or surfactant as suggested by Shen Z. et al.[50] Then, the reaction was placed in a temperature bath depending on the reaction to synthesize the temperature was set at 70 or 50 °C, if the cross-linker was BIS or BAC respectively. To start the polymerization, the initiator APS (0.04 mmol) was added and dissolved in 0.5 mL ultrapure water. It was left reacting for 6 h and purified by dialysis against deionized water for 3 days against ultrapure water, using Spectra–Por 10 kDa MWCO membrane. As has been demonstrated in previous research,[51] reacting at high temperatures can promote the breakdown of the disulfide bonds and the Michael addition between the disulfide bonds and the double bonds, reducing the polymerization efficiency and the degradability of the NG. For this reason, the reaction of p(NIPAM-(S-S)-HEMA)(BIS:BAC) and p(NIPAM-(S-S)-HEMA)(BAC) was carried out at lower temperatures using the TEMED catalyst. The Scheme S1 (Supporting Information) provides additional details regarding the synthesis procedure. The reaction kinetics were characterized by proton-1 nuclear magnetic resonance (^{1}H-NMR) (Figures S2–S6, Supporting Information). In addition, to confirm the successful synthesis and physicochemical properties, the final product was collected, freeze-dried, redispersed if needed, and characterized by ^{1}H NMR spectra (Figure S7, Supporting Information), FTIR (Figure S8, Supporting Information), dynamic light scattering (DLS), scanning electron microscopy (SEM), and atomic force microscope (AFM) (Bruker Dimension ICON) (Figures S9–S11, Supporting Information). The diameters of the nanoparticles from the SEM were extracted using the software ImageJ (Table S6, Supporting Information). For that, 30 nanoparticles were randomly selected and measured using the measurement tool.

Preparation of Rhodamine B Labeled NGs: To prepare Rhodamine B labeled NGs, NGs (1 eq. is referred to as the primary alcohol group) were dispersed in anhydrous DMF, followed by the addition of DCC (1.1 eq.) and Rhodamine B (1.3 eq.) under stirring at 0 °C for 5 min, at that moment DMAP (0.1 eq.) was added dropwise while vigorous stirring to the solution, and it was left to react for 5 h at RT, purification was performed by dialysis (Spectra–Por 10 kDa MWCO membrane) against ultrapure water for various days and the compound was finally collected and freeze-dried for further use.

Thermoresponsive Study: The cloud-point transition temperature (T$_{CP}$) was quantified to study the thermal response of the NGs by measuring

ADVANCED
SCIENCE NEWS
www.advancedsciencenews.com

ADVANCED
FUNCTIONAL
MATERIALS
www.afm-journal.de

the turbidity over temperature. The absorbance at 600 nm was measured using a microplate reader equipped with a temperature control system. The absorbance of NGs dispersions (1 mg mL^{-1}) was measured from 25 to 60 °C with a temperature gradient of 2 °C. Afterward, the transmittance was calculated as follows:

$$\text{Transmitance } (\%) = 10^{(2-\text{Absorbance})} \times 100 \tag{1}$$

Redox-Responsive Study: The chemical reduction was qualitatively determined and compared by Raman spectroscopy, observing the reduction of the disulfide bonds (425—550 cm^{-1}) and the formation of free-thiols (2530—2610 cm^{-1}) mediated by a reductive agent 10 mM TCEP. Chemical reversibility and disulfide formation were observed measuring after 1 week of exposure to air.

DLS and gel permeation chromatography (GPC) were used to characterize degradation at different GSH concentrations over time. For this, solutions of NGs 1 mg mL^{-1} were prepared and incubated in 0, 0.5, 5, and 10.0 mM of GSH for 2, 24 h, and one week after the incubation at 300 r.p.m. Before characterization, GSH was removed by precipitating and redispersing the NGs in water several times by centrifugation. For GPC measurements, OHpal SB-806 M column equipped with OHpak SB-G6B (guard column) was used, ultrapure water was used as mobile phase at a flow rate of 0.4 mL min^{-1}, PDA analyzed the samples at 254 nm. This data was complemented by SEM, cumulant rates measured by DLS using fixed attenuator, >T$_{CP}$ size, and absorbance change after incubating with reductive agents. Further information about the characterization protocols can be found in the supporting information.

Adhesive Force: The determination of the bioadhesive force (F) is important to determine the force of interaction between the material quantitatively and on this case the mucin. As has been observed in other studies,[52,53] this force–energy interaction of the physical and chemical bonds was transformed into mechanical energy causing a change in viscosity. This characterization was expected to demonstrate a strong interaction in the degradable NGs caused by the creation of covalent bonds between the disulfide bonds of the NG and the free thiols present in the mucosa. For the determination of F, 1 mg mL^{-1} NG dispersions in ultrapure water, 1 mg mL^{-1} NG dispersions in a 5 mg mL^{-1} mucin solution, and a 5 mg mL^{-1} mucin solution were prepared. Each of them was characterized rheologically using a constant shear rate of 93 1 s^{-1}, the viscosity was determined at 120 s. As shown in Equation (2), the total viscosity is the sum of the viscosity of the mucin, polymer, and chemical-physical force between the mucin and polymer. Therefore, by estimating the viscosity of the mucoadhesiveness, the bioadhesive force is determined as shown in Equation (3).

$$\eta_{\text{total}} = \eta_{\text{mucin}} + \eta_{\text{polymer}} + \eta_{\text{mucoad}} \tag{2}$$

$$F = \eta_{\text{mucoad}} * \sigma \tag{3}$$

where η_{total} is referred to as the total viscosity; η_{polymer} viscosity of the polymer; η_{mucoad} the viscosity of the mucoadhesion; F bioadhesive force and σ to the shear rate.

Mucus Permeation Study: A mucus permeation study was performed by mucus-modified transwell membranes using a similar protocol proposed by Poinard B. et.al.[54] To modify the membranes, 50 µL of 10% (w/v%) mucus extracted from the small intestine was added to the transwell inserts and allowed to dry for 30 min to generate ≈600 µm mucin layer based on calculation. The mucus-modified transwell inserts were incubated at 37 °C in a 550 µL solution of 10 mM PBS pH = 7.4 at 250 r.p.m. for 10 min. Subsequently, a solution of Rhodamine B labeled NG 10 mg mL^{-1} 50 µL was added to the top. At different time points, the bottom solution was removed and regenerated with fresh PBS. From the extracted solutions, the NG was quantified by fluorescence and the particle permeation is calculated (Equation 4).

$$\text{Particle permeation } (\%) = \frac{\text{NP mucus coated membrane}}{\text{NP tuncoated membrane}} \times 100 \tag{4}$$

Multiple Particle Tracking: To characterize the diffusivity of the different NGs in cystic fibrosis mucus or mucin hydrogels, the multiple particle tracking (MPT) method was employed. The 2% mucin hydrogels were made by first dissolving 20 mg of native mucin from the bovine submaxillary gland (Sigma–Aldrich, Saint Louis, MO, USA) in acetate buffer 0.05 M (pH 5) at 37 °C for 30 min. This was then transferred onto a 10 kDa MWCO Pierce Protein Concentrators PES columns (Thermo Fisher Scientific, Burlington, ON, Canada), centrifuged at 15 000 g for 15 min, washed with Milli-Q water, and then centrifuged again (15 000 g for 15 min). This was repeated three times in total. A final centrifugation was then performed, then the mucin-containing retentate was resuspended at 20 mg mL^{-1} to obtain 2% mucin in Milli-Q water. For mucus samples from cystic fibrosis patients, clinicians at Providence Health Care (Vancouver, BC) made possible the collection of mucus samples which were spontaneously produced by local cystic fibrosis patients at Sant Paul's Hospital, Vancouver, BC, Canada (Ethics approval number: H20-03 198).

For MPT analysis, NGs were added to the mucus/mucin hydrogel in an Ibidi µ-Slide VI-0.4 (Ibidi, Gräfelfing, Germany) at a final volume fraction ≤0.2%. Next, using a PerkinElmer VoX Spinning Disk fluorescence microscope (PerkinElmer, Woodbridge, ON, Canada) equipped with 100× objective, a high-speed Hamamatsu 9100–02 CCD camera and a thermoplate (37 °C), the real-time movement of the NGs in CF mucus/mucin hydrogel was recorded at a frame rate of 10 FPS. At a minimum, 15 videos were recorded per condition, lasting 10 s each. On average 339 NPs were used to determine the median diffusion coefficient in each condition.

The movement of NGs in each video was analyzed using the NanoTrackJ plugin (ImageJ software, Version 1.53k). To start, the spot assistant tool was set to an appropriate tolerance value and mean filter size to maximize the selection of visible NGs while minimizing noise selection. Then, by following the trajectory of each NG, the NanoTrackJ function measured the displacements of each visible NG. Finally, the covariance estimator was employed to estimate the diffusion coefficient of each NG as a function of the measured displacements. According to studies that compared different methods, the covariance method is an unbiased estimation method of diffusivity under different experimental conditions.[55]

Encapsulation and In Vitro Temperature- and/or Redox-Induced Release: The ability of the NGs to encapsulate and release biomacromolecular cargos by a specific stimulus was tested first with fluorescein-labeled albumin as a model protein. BSA is a small, stable, moderately non-reactive protein that is ideal for proof of concept in encapsulation and release studies. For the encapsulation of the NGs, a solution of BSA-FITC (2 mg mL^{-1}) was prepared, this solution was added to the freeze-dried NG in a weight ratio of 2:1 NG:BSA FITC, and stored overnight at 4 °C. The free protein was separated by a few cycles of vivaspin centrifugal concentrator 300 kDa MWCO, the free protein was characterized at 280 nm. A calibration curve was made using different concentrations of BSA-FITC and the encapsulation efficiency (EE) (Equation 5) and loading capacity (LC) (Equation 6) were calculated.

$$EE(\%) = \frac{\text{Model protein}_{\text{Loaded}}}{\text{Model protein}_{\text{Initial}}} \times 100 \tag{5}$$

$$LC(\%) = \frac{\text{Model protein}_{\text{Loaded}}}{\text{Model protein}_{\text{Total}}} \times 100 \tag{6}$$

BSA-FITC Release Studies by Ex Vivo Small Intestine Model: A local slaughterhouse kindly provided fresh calf small intestine from a healthy animal. The calf was slaughtered for a commercial meat production process. Therefore, no ethical requirements specific to this study were necessary. The fresh intestinal segments were carefully opened longitudinally, frozen in liquid nitrogen, stored at −20 °C, and defrosted overnight in the fridge before use. For the ex vivo experiment, a piece of 3 cm × 3 cm calf small intestine was placed in a Petri dish with a wetted soft paper on the bottom. A plastic cylinder of 2 cm in diameter was driven into the tissue to act as a sample container. Afterward, 300 µL of FITC-loaded- NG suspension (1 mg mL^{-1} BSA-FITC-1 mg mL^{-1} NGs) was placed into the cylinder container. The Petri dish containing the sample was incubated at 37 °C

for 2 h. After incubation, the tissue pieces were fixed by immersion in 4% paraformaldehyde for 24 h, then kept 24 h in 15% sucrose and 24 h in 30% sucrose for cryoprotection. Afterward, the samples were embedded in OCT media to cut 30 µm-cryosections using a cryostat (CM3050 S Leica Microsystems GmbH, Weltzar, Germany). The tissue sections were analyzed using an inverted Nikon Eclipse Ti2 – Fluorescence microscope. The fluorescence intensity of the penetrated protein in the mucosal layer was quantified as integrated density using ImageJ Software.

The penetration of FITC-loaded-Rhodamine B labeled NGs across the mucosal barrier was also studied. For this in vitro experiment, the mucus was carefully removed from the tissue using a spatula. Then, 130 mg of mucus was placed per well of a glass chamber (Lab-Tek) and let dry overnight at room temperature in the hood. After that, 100 µL of FITC-loaded-Rhodamine B labeled NG suspension (1 mg mL^{-1} Rhodamine B labeled NGs-1 mg mL^{-1} BSA FITC) was added into the well and incubated for 2 h at 37 °C with and without 10 mM of GSH. After incubation, the wells were observed at different z planes in the green and red channels using an inverted Nikon Eclipse Ti2 – Fluorescence microscope. The data were analyzed using ImageJ software and reported as a z-axis profile of green and red channels.

Cell Uptake: The cellular uptake of Rhodamine B labeled NGs was visualized by EVOS M5000 Imaging System (Thermo Fisher Scientific, Burlington, ON, Canada). Primary human bronchial epithelial cells (HBE) were seeded in a sterile 12-well plate at 100 000 cells per well overnight at 37 °C and 5% CO$_2$ and then treated with NGs diluted to 1 mg mL^{-1} in culture medium. After 4 h, the media was aspirated from the wells, and cells were washed with PBS. The nuclei were stained by Hoechst 33342 Solution (Thermo Fisher Scientific CatNr. 62249, 1:2000 dilution). The cells were then imaged using the EVOS M5000 Imaging System (Thermo Fisher Scientific, Burlington, ON, Canada).

Cell Viability: The cytotoxicity of the NGs was assessed via the 3-(4,5-dimethylthiazol-2-yl)-2,5-diphenyl tetrazolium bromide (MTT) assay. First, 20 000 HBE cells were seeded in a 96-well plate for 24 h to reach ≈70% confluence. Then, the cells were treated with 1 mg mL^{-1} NGs in culture media at 37 °C and 5% CO$_2$ for 24 h. As a untreated (healthy) control, the cells were incubated in the growth media;, as cytotoxic control, the cells were incubated in 10% DMSO solution. Next, the media with NGs were aspirated from the wells, and MTT at 0.5 mg mL^{-1} in culture media was added to each well and then incubated for 4 h at 37 °C and 5% CO$_2$. After that, the insoluble formazan crystals were dissolved in 50 µL DMSO and quantified using the Bio-Tek µQuant.

C. elegans Studies: NGs were dispersed in ultrapure water at 1 mg ml^{-1} concentration and kept at 4 °C until further use. Before their evaluation, they were left for 15 min at RT to warm up. Worms were synchronized at the L4 stage to start the evaluation following previous protocols.[46] An average number of 15 ± 3 L4 worms were transferred to 96-well plates per well. The final exposure volume was 100 µL of 3 µL worms in M9 buffer, 4 µL of heat inactivated-*E. coli* OP50 (OD$_{600}$ = 1 × 2.5 concentrated), 43 µL M9 buffer, and 50 µL of 1 mg mL^{-1} NG solution to have a final concentration of 0.5 mg mL^{-1} of each. As a negative control, ultrapure water was used, as NGs were dissolved in it, and 5% dimethyl sulfoxide (DMSO) in ultrapure water was used as a positive control.

Worms were exposed for 24 h in these conditions at 20 °C, and the survival rate was immediately measured. N = 3 n = 540. Data represents the mean ± SEM. Then, worms were washed of NGs with three rounds of 1 min at 1300 x g, and the supernatant was replaced with fresh M9 buffer. Worms were paralyzed with 10 mM sodium azide and imaged to measure the length of worms. N = 3 n = 150. Data represents mean ± SD. Worms were also imaged with an Olympus BX51 optical microscope coupled to a fluorescent lamp to determine the biodistribution of nanogels. Rhodamine B was excited with a 510–550 nm light, and emission was observed at 590 nm. BSA-FITC was excited with a 450–480 nm filter and observed at 515 nm.

To assess the clearance of NGs from worms, treated worms were transferred to fresh OP50-seeded NGM plates and left for 5 h at 20 °C. Afterward, worms were recollected with M9 buffer and cleaned thrice to remove bacteria. Each clean step consisted of 1 min at 1300 x g and replacing supernatant with fresh M9 buffer.

Confocal Microscopy of C. elegans: Confocal analysis was performed just after the exposure. Worms were cleaned and anesthetized as described above. Worms were directly placed onto a microscope slide and covered with a cover slide. Leica TCS SP8 confocal multispectral microscope with STED 3× and HyVolution at Sant Joan de Deu Hospital (Barcelona) was used. A total of 5 worms were imaged for further analysis.

ImageJ/Fiji (Image J 1.54f version) was chosen for quantification analysis. As the green channel was saturated, quantification was performed by analyzing the red fluorescence, corresponding to the Rhodamine B molecules covalently attached to NGs. Working in the red channel, a 2D Z-sum projection was created, and intensity was measured per area (µm2) of worms. All images were calibrated to have a maximum intensity signal and plotted with a Royal lookup table in ImageJ to better see the differences in intensity.

The number of spheres that cross the intestinal barrier was checked using the function 3D Object Counter (Analyze).[49] The threshold of each image was selected manually, and the size was limited to a minimum of 10 voxels and a maximum of 100 voxels to avoid the intestinal lumen region. The area and number of particles were counted.

The plugin JACOP, with the method based on Lachmanivich et al. and the object-based method, was applied to avoid considering the fluorescent intensity.[56] Two channels colocalization was considered when the object's mass center of the red channel was in the object's area of the green channel. Values of colocalization go from 0 to 100%. In the case of this study, a low grade of colocalization corresponds with a good release of the cargo molecule (BSA-FITC in green) from the NG (Rhodamine B-red).

Statistical Analysis: Experimental data were given as the mean ± standard deviation (SD). The one-way analysis of variance method was adopted to evaluate the significance level of the experimental data between groups through Graphpad Prism 9. A p value of 0.05 was selected as the significance level, and all data were marked as * for $p < 0.05$, ** for $p < 0.01$, and *** for $p < 0.001$.

Supporting Information

Supporting Information is available from the Wiley Online Library or from the author.

Acknowledgements

Conflict of Interest

The authors declare no conflict of interest.

Author Contributions

J.U. and M.C. conceived the idea and project. J.U. synthesized, optimized, and characterized by DLS, Z-potential, H-NMR, etc. the NGs. J.U. optimized the protein encapsulation and performed the release studies. J.U. performed mucin/mucus experiments and M.S.O. performed mucus tissue penetration study. A.M. and A.L. performed *C.elegans* in vivo studies characterization and analysis. B.T. and S.H. performed mucus diffusivity assays, analysis, and characterization of cell studies. J.U. wrote the first draft of the manuscript and M.S.O and M.C. revised and improved it. M.C. supervised the work and was responsible for funding. All authors have revised and approved the final version of the manuscript. The authors declare that they have no competing interests.

Data Availability Statement

The data that support the findings of this study are available from the corresponding author upon reasonable request.

Keywords

[1] M. M. France, J. R. Turner, *J. Cell Sci.* **2017**, *130*, 307.
[2] T. Oshima, H. Miwa, *J. Gastroenterol.* **2016**, *51*, 768.
[3] M. O. Henke, F. Ratjen, *Paediatr. Respir. Rev.* **2007**, *8*, 24.
[4] K. F. Csáki, *Med. Hypotheses* **2011**, *76*, 676.
[5] M. Ghadiri, P. M. Young, D. Traini, *Pharmaceutics* **2019**, *11*, 113.
[6] R. Bansil, B. S. Turner, *Adv. Drug. Deliv. Rev.* **2018**, *124*, 3.
[7] A. P. Moran, A. Gupta, L. Joshi, *Gut* **2011**, *60*, 1412.
[8] M. A. McGuckin, S. K. Lindén, P. Sutton, T. H. Florin, *Nat. Rev. Microbiol.* **2011**, *9*, 265.
[9] N. A. Hering, M. Fromm, J.-D. Schulzke, *J. Physiol.* **2012**, *590*, 1035.
[10] H. J. Forman, H. Zhang, A. G. Rinna, *Mol. Aspects Med.* **2009**, *30*, 1.
[11] N. Dauletbaev, K. Viel, R. Buhl, T. O. F. Wagner, J. Bargon, *J. Cyst. Fibros.* **2004**, *3*, 119.
[12] G. Wu, J. R. Lupton, N. D. Turner, Y.-Z. Fang, S. Yang, *J. Nutr.* **2004**, *134*, 489.
[13] H. Hosseinkhani, *Nanomaterials in Advanced Medicine*, Wiley, Hoboken, NJ, USA **2019**.
[14] H. Hosseinkhani, *Biomedical Engineering: Materials, Technology, and Applications*, Wiley, Hoboken, NJ, USA **2022**.
[15] P. Schattling, E. Taipaleenmäki, Y. Zhang, B. Städler, *Macromol. Biosci.* **2017**, *17*, 1700060.
[16] S. Haddadzadegan, P. Knoll, R. Wibel, G. Kali, *Acta Biomater.* **2023**, *167*, 309.
[17] J. C. Cuggino, E. R. O. Blanco, L. M. Gugliotta, C. I. Alvarez Igarzabal, M. Calderón, *J. Control. Release* **2019**, *307*, 221.
[18] R. Charbaji, M. Kar, L. E. Theune, J. Bergueiro, A. Eichhorst, L. Navarro, P. Graff, F. Stumpff, M. Calderón, S. Hedtrich, *Small* **2021**, *17*, 202007963.
[19] F. Abedini, M. Ebrahimi, A. H. Roozbehani, A. J. Domb, H. Hosseinkhani, *Polym. Adv. Technol.* **2018**, *29*, 2564.
[20] C. Gelfi, A. Alloni, P. de Besi, P. G. Righetti, *J. Chromatogr. A* **1992**, *608*, 343.
[21] M. Dirksen, P. Fandrich, L. Goett-Zink, J. Cremer, D. Anselmetti, T. Hellweg, *Langmuir* **2022**, *38*, 638.
[22] R. A. Cone, *Adv. Drug Deliv. Rev.* **2009**, *61*, 75.
[23] S. Ghaeini-Hesaroeiye, H. R. Bagtash, S. Boddohi, E. Vasheghani-Farahani, E. Jabbari, *Gels* **2020**, *6*, 20.
[24] J. Beier, K. M. Beeh, D. Semmler, N. Beike, R. Buhl, *Ann. Allergy Asthma Immunol.* **2004**, *92*, 459.
[25] L. C. Lands, V. Grey, A. A. Smountas, V. G. Kramer, D. McKenna, *Chest* **1999**, *116*, 201.
[26] Y. Men, S. Peng, P. Yang, Q. Jiang, Y. Zhang, B. Shen, P. Dong, Z. Pang, W. Yang, *ACS Appl. Mater. Interfaces* **2018**, *10*, 23509.
[27] L. Zhang, H. Xue, Z. Cao, A. Keefe, J. Wang, S. Jiang, *Biomaterials* **2011**, *32*, 4604.
[28] A. D. Permana, E. Utomo, M. R. Pratama, M. N. Amir, Q. K. Anjani, S. A. Mardikasari, S. Sumarheni, A. Himawan, A. Arjuna, U. Usmanengsi, R. F. Donnelly, *ACS Appl. Mater. Interfaces* **2021**, *13*, 18128.
[29] L. D. Li, T. Crouzier, A. Sarkar, L. Dunphy, J. Han, K. Ribbeck, *Biophys. J.* **2013**, *105*, 1357.
[30] J. Leal, H. D. C. Smyth, D. Ghosh, *Int. J. Pharm.* **2017**, *532*, 555.
[31] X. Li, Q. Li, C. Zhao, *ACS Omega* **2021**, *6*, 13774.
[32] N. Morgulchik, N. Kamaly, *ACS Appl. Nano Mater.* **2021**, *4*, 4256.
[33] W. Huang, C. P. Tsui, C. Y. Tang, L. Gu, *Sci. Rep.* **2018**, *8*, 13002.
[34] S. P. Bandi, S. Bhatnagar, V. V. K. Venuganti, *Acta Biomater.* **2021**, *119*, 13.
[35] C. Gerecke, A. Edlich, M. Giulbudagian, F. Schumacher, N. Zhang, A. Said, G. Yealland, S. B. Lohan, F. Neumann, M. C. Meinke, N. Ma, M. Calderón, S. Hedtrich, M. Schäfer-Korting, B. Kleuser, *Nanotoxicology* **2017**, *11*, 267.
[36] P. Knoll, G. Francesco Racaniello, V. Laquintana, F. Veider, A. Saleh, A. Seybold, N. Denora, *Int. J. Pharm.* **2023**, *635*, 122753.
[37] P. Kanjilal, K. Dutta, S. Thayumanavan, *Angew. Chem., Int. Ed.* **2022**, *61*, e202209227.
[38] V. Forest, J. Pourchez, *Mater. Sci. Eng., C* **2017**, *70*, 889.
[39] C. R. Miller, B. Bondurant, S. D. McLean, K. A. McGovern, D. F. O'Brien, *Biochemistry* **1998**, *37*, 12875.
[40] S. E. A. Gratton, P. A. Ropp, P. D. Pohlhaus, J. C. Luft, V. J. Madden, M. E. Napier, J. M. DeSimone, *Proc. Natl. Acad. Sci. USA* **2008**, *105*, 11613.
[41] I. Ruseska, A. Zimmer, *Beilstein J. Nanotechnol.* **2020**, *11*, 101.
[42] A. Verma, F. Stellacci, *Small* **2010**, *6*, 12.
[43] O. Lunov, T. Syrovets, C. Loos, J. Beil, M. Delacher, K. Tron, G. U. Nienhaus, A. Musyanovych, V. Mailänder, K. Landfester, T. Simmet, *ACS Nano* **2011**, *5*, 1657.
[44] L. Gonzalez-Moragas, A. Roig, A. C. Laromaine, *Adv. Colloid Interface Sci.* **2015**, *219*, 10.
[45] J. Schimpf, K. Sames, R. Zwilling, *Histochem. J.* **1999**, *31*, 285.
[46] S. Rojas, T. Hidalgo, Z. Luo, D. Ávila, A. Laromaine, P. Horcajada, *ACS Nano* **2022**, *16*, 5830.

ADVANCED
SCIENCE NEWS
www.advancedsciencenews.com

ADVANCED
FUNCTIONAL
MATERIALS
www.afm-journal.de

[47] M. Weiss, J. Fan, M. Claudel, T. Sonntag, P. Didier, C. Ronzani, L. Lebeau, F. Pons, *J. Nanobiotechnol.* **2021**, *19*, 5.

[48] S. K. Hanna, G. A. Cooksey, S. Dong, B. C. Nelson, L. Mao, J. T. Elliott, E. J. Petersen, *Environ. Sci. Nano* **2016**, *3*, 1080.

[49] S. Bolte, F. P. Cordelières, *J. Microsc.* **2006**, *224*, 213.

[50] Z. Shen, A. Mellati, J. Bi, H. Zhang, S. Dai, *RSC Adv.* **2014**, *4*, 29146.

[51] M. Mackiewicz, J. Romanski, E. Drozd, B. Gruber-Bzura, P. Fiedor, Z. Stojek, M. Karbarz, *Int. J. Pharm.* **2017**, *523*, 336.

[52] E. H. Emad, M. G. James, *Pharm. Res.* **1990**, *7*, 491.

[53] S. Mansuri, P. Kesharwani, K. Jain, R. K. Tekade, N. K. Jain, *React. Funct. Polym.* **2016**, *100*, 151.

[54] B. Poinard, S. Kamaluddin, A. Q. Q. Tan, K. G. Neoh, J. C. Y. Kah, *ACS Appl. Mater. Interfaces* **2019**, *11*, 4777.

[55] C. L. Vestergaard, P. Blainey, H. Flyvbjerg, *Biophys. J.* **2013**, *104*, 174a.

[56] F. P. Cordelì, S. Bolte, F. P. A guided tour into subcellular colocalization analysis in light microscopy, *J. Microsc.* **2006**, *224*, 213.

2407044 (15 of 15)